Numerical and Experimental Study of Damped Oscillating Manometers: II. Non-Newtonian Fluids

JOHN C. BIERY

University of Wisconsin, Madison, Wisconsin

To test the importance of visco-elastic properties of non-Newtonian fluids in an oscillatory system of low frequency the dynamic characteristics of a series of non-Newtonian fluids were studied in oscillating manometers. The manometer fluid behavior was simulated on a digital computer by numerically integrating the axial component of the equation of motion. In the simulation cone and plate steady state rheological data were represented mathematically with the Sisko rheological model. Good agreement between simulation and experimental data was obtained. This agreement implies that steady state rheological models can be utilized in the description of unsteady state non-Newtonian systems where the characteristic period of the system is many times greater than the relaxation and retardation times of the fluid. When this characteristic period approaches these times, then rheological models which incorporate visco-elastic terms explicitly probably should be used.

Non-Newtonian fluids when tested under various experimental conditions exhibit different types of phenomena. As these phenomena were observed and tested, various rheological models were developed to describe the behavior. For instance steady state experiments in capillary tube, concentric cylinder, and cone and plate viscometers produced nonlinear shear stress vs. rate of shear curves. To describe this effect generalized Newtonian models such as the power law, Ellis, Sisko, Eyring, Reiner-Philippoff models were developed (*1*). These formulations however were not able to describe the normal stress behavior seen in the Weissenberg effect and in the normal stress cone and plate experiments. As a result the more general Reiner-Rivlin-Prager rheological model was evolved (*2*). Other experiments were run in which non-Newtonian fluids were oscillated at high frequencies in cup and piston or oscillating concentric cylinder experiments (*3*). For small oscillations linear visco-elastic theory was employed to describe the phenomena (*4*). To include in the mathematical formulations the anomalous behavior observed in these experiments and the others cited above the nonlinear visco-elastic models of Oldroyd and Rivlin-Erickson were postulated (*5, 6*).

In engineering design of systems containing non-Newtonian fluids the simplest of the above models which will adequately describe the phenomena of interest should be used. In many design problems the conditions do not exactly correspond to the experimental circumstances under which the rheological model was developed. For instance in unsteady state processes where there are slow oscillations or slowly changing transient conditions the applicability of the various models is not known. Can the steady state rheological models be used to simulate such unsteady state processes, or must the nonlinear visco-elastic models be utilized?

To test the usefulness of the steady flow rheological models under transient conditions the dynamic characteristics of a series of non-Newtonian fluids were studied in the oscillating manometer system. The experimental oscillating manometer data were simulated by numerically integrating the axial component of the equation of motion in cylindrical coordinates. The Sisko rheological model which expresses shear stress as an explicit function of shear rate and which also contains a lower limiting viscosity was utilized in the simulation. Fourteen experiments were run in three diameter manometers with six non-Newtonian fluids. The numerical simulation procedure was modified by end-effect corrections developed previously to simulate Newtonian fluid behavior in these manometers (*7*). The resulting simulation damping factors and cycle times were compared with the experimental data, and the deviations were analyzed statistically. The statistical comparison of the Newtonian and non-Newtonian simulations indicated that the steady state model did adequately describe the oscillatory behavior of the non-Newtonian fluids in the manometers.

EXPERIMENTAL EQUIPMENT, PROCEDURE, AND RESULTS

Equipment Description and Experimental Procedure

The experimental equipment and experimental procedure utilized are the same as described in the Newtonian oscillating manometer paper (*7*). Therefore only a brief description of the equipment and procedure is presented below. The dimensions and configuration of the three glass tube manometers used in the experiments are indicated in Figure 1 and in Table 1.

John C. Biery is at the University of California, Los Alamos Scientific Laboratory, Los Alamos, New Mexico.

The dynamics of the manometer were studied by initially forcing the legs of fluid into a position of imbalance and then allowing the fluid to oscillate freely by removing the restraining force. The cycle times and maximum amplitudes were measured after the first one half cycle and every full cycle thereafter.* The legs were forced into a position of imbalance by applying air pressure to the right-hand leg with an air hose connected to a rubber stopper. By quickly removing the stopper the fluid was allowed to oscillate. Some added damping occurred in the first ½ cycle owing to the outward flow of the compressed air in the right leg.† However after this initial cycle the flow of air in the manometer caused negligible damping of the oscillating fluid.

The oscillation cycle times were measured by manually starting an electric stop watch at the start up of the fluid and stopping it at the maximum in amplitude for the cycle of interest. Also the amplitude of each oscillation was measured by adjusting rubber bands on the outside of the tube to correspond to the maximum and minimum position of the liquid meniscus in each leg for each cycle. A complete description of the procedure and the errors involved is presented in the Newtonian manometer paper (7). A summary of the standard deviations and confidence intervals for the measured cycle times is presented in Table 2. No statistical replications for the height measurements were made; however the errors involved in the measurements were believed to be less than ±1% for heights greater than 5 cm. and ± 0.05 cm. for heights below 5 cm.

For comparison with the reported data in dimensionless time units Table 3 gives the equivalence of dimensionless time to real time for the three manometers.

Rheological Measurements

A critical experimental measurement was the determination of the steady state flow rheological curve for each non-Newtonian fluid studied. The curves of shear stress vs. rate of shear can be found by capillary tube flow measurements or by torque measurements in concentric cylinder or cone and plate viscometers. For this experiment a Ferranti-Shirley cone and plate viscometer was used. After the development of a reliable experimental procedure (*10*) the torque values for a given shear rate were found to be accurate to within ± 2% for Newtonian fluids with viscosities near 0.5 poise.

Three of the non-Newtonian fluids, 0.3% Natrosol-Hi, 1.0 Natrosol-Med., and 0.8% Polyox,** had relatively low viscosities, and as a result, the rheological curves determined were less accurate than indicated by the ± 2% limit. For these fluids the torque measuring instrument registered maximum readings of from 7 to 12 units on a 100 unit scale for the maximum cone speed of 100 rev./min. Also the maximum rate of shear in the manometer corresponded to a maximum rate of rotation of 10 rev./min. or a rate of shear of 173 sec.$^{-1}$. For these fluids the curve in this region was somewhat uncertain and probably could have been in error by as much as ± 10 to 20%. The simulation results indicate that the experimental rheological curves for 0.3% Natrosol-Hi and 1.0% Natrosol-Med. had apparent measured viscosities which were somewhat too large. A similar determination on a Newtonian fluid, approximately 50% glycerine in water, in this shear stress range produced a viscosity which was approximately 9% high.

The rheological curves for the polymer solutions were determined five days or less after the actual manometer experiments were run. All solutions except 0.8% Polyox were quite stable as indicated by repeated determinations on the cone and plate viscometer. The 0.8% Polyox solution was slowly degrading, and as a result the rheological curve determined was somewhat inaccurate for Run 27 in the 1.256-cm. tube. The experimental rheological curves are shown in Figures 2 and 3.

Two models, Sisko and a steady state modified Oldroyd model (*11*), were fitted to the rheological data. The constants for the equations are given in Table 4. The formulas for the models are presented in Equations (1) and (2).

Sisko model:

$$\tau_{rz} = \eta_0 \frac{dv_z}{dr} + \beta \left| \frac{dv_z}{dr} \right|^{m-1} \frac{dv_z}{dr} \qquad (1)$$

Oldroyd 3 constant model:

$$\tau_{rz} = -\eta_0 \left(\frac{dv_z}{dr}\right) \frac{1 + 2/3\,\lambda_1\lambda_2 \left(\frac{dv_z}{dr}\right)^2}{1 + 2/3\lambda_1^2 \left(\frac{dv_z}{dr}\right)^2} \qquad (2)$$

The zero rate of shear limiting viscosity is η_0 in the above equations. This viscosity was measured by estimating the initial slope on the shear stress vs. rate of shear curve. This slope was obtained by drawing a tangent line to the curve at zero rate of shear.* The other constants were obtained by forcing the model to match the experimental curve at 86.5 and 173 sec.$^{-1}$ rate of shear. As indicated by Williams and Bird (*11*) λ_1 and λ_2 are stress relaxation and shear retardation times from the original Oldroyd model. These constants probably give an estimate of the time over which visco-elastic effects may be important after some change in shear rate or shear stress is made. In Figures 4 and 5 are shown the experimental and Sisko model simulation shear stress rate of shear curves.

The simple power law model was considered to be inadequate for the manometer simulation because the model does not produce a nonzero lower limiting viscosity. Since the rate of shear in the manometer was low at small amplitudes and at the end of each cycle, the viscosity prediction in the low shear rate range was very important. As is shown in Figures 4 and 5 the Sisko model simulated the experimental data very well in this low range.

Experimental Conditions and Results

In Table 5 are listed the experimental conditions for each manometer run. Also in Table 10 in the Appendix† can be found the amplitudes, cycle times, and damping factors** for the manometer runs.

MATHEMATICAL SIMULATION

The mathematical simulation procedure was very similar to that used in the Newtonian manometer simulations

* One full cycle period is the time required for the legs to return to a maximum position similar to the initial position. A half cycle period is the time required to attain a minimum position with the legs reversed to the initial position.

† The outrush of the air produced a force against the depressed liquid leg. The effect was much like that when air is allowed to exit rapidly from a rubber balloon. The reaction force from the air efflux actually tended to depress the manometer leg even farther. Calculations show that this force existed over a period of approximately 2 × 10^{-5} sec. and developed approximately 1 atm. of reaction pressure.

** Natrosol-Hi, Type H. A high molecular weight water soluble polymer of hydroxymethyl cellulose. Natrosol-Medium Type G. A medium molecular weight water soluble polymer of hydroxymethyl cellulose. Polyox type WSR-301. A high molecular weight water soluble polymer of ethylene oxide.

* The errors in this measurement are uncertain. With lower viscosity solutions the possible error was greater owing to the insensitivity of the cone and plate viscometer in the low torque range. Some lower limiting viscosities from similar concentration solutions were determined by falling ball techniques. As compared with these values the graphical lower limiting viscosities were from 5 to 17% low for fluids above 1.0 poise. For fluids near 0.2 to 0.3 poise graphical lower limiting viscosity readings were 23 to 28% high.

† The Appendix to this paper has been deposited as document 7970 with the American Documentation Institute, Photoduplication Service, Library of Congress, Washington 25, D. C., and may be obtained for $2.50 for photoprints or $1.75 for 35-mm. microfilm.

** The amplitude decrement data were analyzed by applying the standard second-order damped harmonic differential equation solution to each half cycle (9). Thus if this equation did not apply over the whole time range, the damping factor would vary from cycle to cycle. The differential equation is as follows:

$$\frac{d^2h^*}{dt^{*2}} + 2\omega_n\zeta \frac{dh^*}{dt^*} + \omega_n^2 h^* = 0$$

where ζ is the damping factor, and ω_n is the natural frequency of the system. This equation has the following underdamped solution:

$$h^* = \frac{h_0^*}{\omega} e^{-\zeta t^*} \omega_n \left[\sin\left(\omega\omega_n t^* + \tan^{-1}\frac{\omega}{\zeta}\right)\right]; \quad \omega = \sqrt{1-\zeta^2}$$

When the amplitudes of the harmonic motion are known, the damping factor can be calculated from the following equation:

$$\frac{\zeta^2}{1-\zeta^2} = \left[\frac{1}{n\pi} \ln\left(\left|\frac{h^*_a}{h^*_b}\right|\right)\right]^2$$

n = number of half cycles between height measurements h^*_a and h^*_b.

(7). The major change in the procedure was the utilization of a nonlinear shear stress rate of shear rheological function in the equation of motion and its finite difference approximation. The simulation was achieved by numerically integrating the z component of the equation of motion in cylindrical coordinates. This integration produced radial velocity profiles which were assumed to exist at all longitudinal positions not close to the ends of the fluid columns. The assumptions of the integration are that $v_r = 0$, $v_\theta = 0$, and $v_z = v_z(r, t)$.* In the manometer the forcing function term $\left(-\frac{\partial P}{\partial z} + \rho g_z \right)$ is equal to $\frac{-2\rho g h}{L}$ when only the imbalance of the liquid legs is the driving force. However, as pointed out in the Newtonian manometer paper, additional end effect terms due to flow reversal at the ends of the liquid legs and surface tension must be subtracted from the basic driving force to adequately represent the dynamic behavior of a manometer fluid. In this case where the fluid wets the glass tube, only the flow reversal end effect need be included.† With the end effect included the equation of motion assumes the following form:

$$\rho \frac{\partial v_z}{\partial t} = -\frac{2\rho g h}{L} - \frac{F_T}{L} - \frac{1}{r} \frac{\partial (r \tau_{rz})}{\partial r} \tag{3}$$

$$\tau_{rz} = -\eta_0 \left(\frac{\partial v_z}{\partial r} \right) + \beta \left| \frac{\partial v_z}{\partial r} \right|^{m-1} \left(\frac{\partial v_z}{\partial r} \right) \tag{4}$$

$$F_T = K_T S r_0 \langle v_z \rangle \eta_{r=r_0} \tag{5}$$

$$\eta_{r=r_0} = \left(\eta_0 - \beta \left| \frac{\partial v}{\partial r} \right|^{m-1} \right)_{r=r_0} \tag{6}$$

The dimension z is taken along the center line of the tube and is positive in an upward direction in the left hand tube (Figure 1). Also the liquid levels in the two legs indicated by h_1 for the left leg and h_2 for the right leg are positive in the directions shown in Figure 1. In this analysis the effect of the film of liquid left adhering to the sides of the manometer tube is ignored, and therefore h in the above equations equals $(h_1 + h_2)/2$.

For the reversal end effect correction made in the Newtonian manometer work the viscosity was of course constant and did not vary as the shear rate varied. However to incorporate this correction into the non-Newtonian equations some characteristic non-Newtonian viscosity had to be selected for the end effect term. Arbitrarily the viscosity associated with the rate of shear at the wall of the tube was selected.

In dimensionless form the equations appear as follows:

$$\left(\frac{\partial v_z^*}{\partial t^*} \right) = -\frac{4}{3} \frac{h^*}{L^*} - \frac{F_T^*}{L^*} - \frac{1}{r^*} \frac{\partial (r^* \tau_{rz}^*)}{\partial r^*} \tag{7}$$

$$\tau_{rz}^* = -\frac{1}{6\Omega_1} \left(\frac{\partial v_z^*}{\partial r^*} \right) + \frac{1}{6\Omega_4} \left| \frac{\partial v_z^*}{\partial r^*} \right|^{m-1} \left(\frac{\partial v_z^*}{\partial r^*} \right) \tag{8}$$

$$F_T^* = \frac{4}{3} \langle v_z^* \rangle \eta^* \Omega_2 \tag{9}$$

From the velocity profile the average velocity of the fluid column can be found by integrating the velocity over the cross-sectional area of the tube. The integration in dimensionless variables is as follows:

$$\frac{dh^*}{dt^*} = \langle v_z^* \rangle = 2 \int_0^1 v_z^* \, r^* \, dr^* \tag{10}$$

The integration of the above equations can be accomplished numerically in a manner similar to that outlined in the Newtonian manometer paper (7). The general procedure includes a calculation of the velocity profile at a given time from which the instantaneous overall velocity of the fluid column is obtained by integration across the radius of the tube. The change of position of the manometer column is obtained by applying this average velocity

* These assumptions ignore the effect of the curved section in the manometer. The curvature forces some fluid to flow radially. By making a large radius curve this effect was minimized. The smaller the ratio r_0/R, the smaller is the effect.
The size of the curvature effect was investigated with the use of a correlation in Goldstein (15). For the fluids used in these experiments the curvature effect was found to be negligible.

† The flow-reversal end effect force resulted from the reversal of the flow stream lines at the ends of the fluid columns. This effect was arbitrarily included in the equation of motion as shown in Equation (3). The work reported in the Newtonian paper showed that Kr_0 was fairly independent of tube radius and fluid properties and equalled 70.4 cm.$^{-1}$. In the non-Newtonian simulations this value of Kr_0 was arbitrarily used in the flow reversal end effect correction.

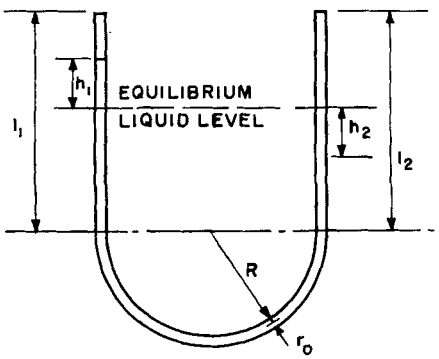

Fig. 1. Manometer with characteristic dimensions.

Table 1. Manometer Tube Dimensions

Tube no.	Straight section length, cm. l_1	l_2	Bend radius, cm.	Tube inside radius, cm. Straight section	Curved section	Total length along center line, cm.
1	32.45	28.60	19.69	1.267	1.251	122.89
2	30.28	30.28	20.04	1.078	1.052	123.52
3	31.90	30.25	19.53	0.4602	0.4545	123.51

Table 2. Confidence Intervals and Standard Deviations of Cycle Time Measurements

Period measured	Average standard deviation of mean cycle time, sec.	Average 90% confidence interval of mean cycle time, sec.
1st half cycle	0.012	±0.035
1st full cycle	0.010	±0.03
2 cycles minus 1 cycle	0.016	±0.04
3 cycles minus 2 cycles	0.018	±0.05
4 cycles minus 3 cycles	0.020	±0.06
5 cycles minus 4 cycles	0.020	±0.06

TABLE 3. EQUIVALENT DIMENSIONLESS TIME UNITS

Manometer number	Radius, cm.	Number of units equivalent to 0.01 sec.
1	1.25	0.34
2	1.05	0.37
3	0.45	0.57

over the next time increment. Convergence properties of the procedure are similar to those found for the Newtonian manometer calculations.

Simulation Results

A complete tabulation of the computer simulations is presented in Table 11 in the Appendix.* A comparison of the simulation results corrected for truncation errors with experimental results is shown in Table 7 in the Appendix.*

VELOCITY PROFILES

The computed velocity profiles have the same distorted shapes that were evidenced in the Newtonian runs (7). As an example of this distortion a series of profiles that were computed in Run 29 are shown in Figures 6 and 7. Since the fluid in Run 29 was relatively viscous as compared with water, the profiles approached a flattened parabolic profile in the center portion of the stroke. However at the ends of the stroke the fluid at the wall tended to reverse direction before the main body of fluid reversed. This effect produced waves in the velocity profile which traveled inward toward the center of the tube. As a result, at least for the more dilute polymer solutions, the effect of a previous stroke tended to shape the profile of one and possibly two succeeding strokes before its particular distortion wave tended to smooth out.

In Figures 6 and 7 the computed radial velocity profiles at various time intervals are presented. These calculated profiles are believed to approximate the actual profiles at all longitudinal positions away from the ends of the fluid legs. On the right side of the figures are shown the fluid position and its direction of movement.

It should be noted that the computed shapes of the velocity profiles have not been verified experimentally.

* See footnote on page 552.

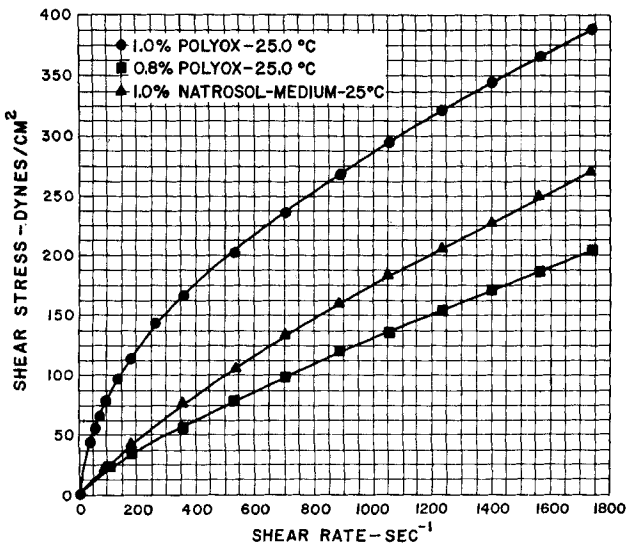

Fig. 2. Experimental rheological curves from cone and plate viscometer.

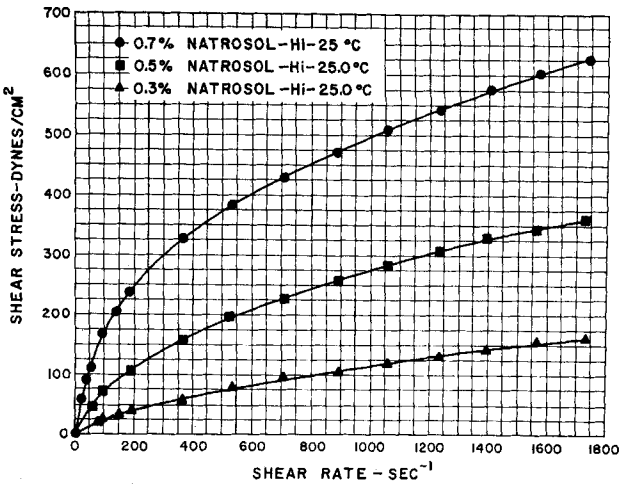

Fig. 3. Experimental rheological curves from cone and plate viscometer.

The integrated behavior with these profiles reproduce the experimental cycle times and damping factors quite satisfactorily. However this agreement is only an indirect proof that the experimental profiles are so formed.

RESULTS AND CONCLUSIONS

In Table 7 in the Appendix* is presented a complete per cycle comparison of the simulated and experimental damping factors and cycle times. The comparison was made on a per cycle basis since the damping factors and cycle times increased as the amplitude of the manometer motion decreased, and as a result the rate of shear of the fluid also decreased. This increase in damping factors and cycle times was observed experimentally and was reproduced in the mathematical simulation. The final comparisons between the experimental and simulated values were made with the reversal end effect included, and the differences were expressed numerically by calculating the percentage error between the two values. To determine whether or not visco-elastic effects were evident in the manometer behavior the error data for the Newtonian and non-Newtonian runs were compared statistically by hypothesis testing methods.

* See footnote in column 1.

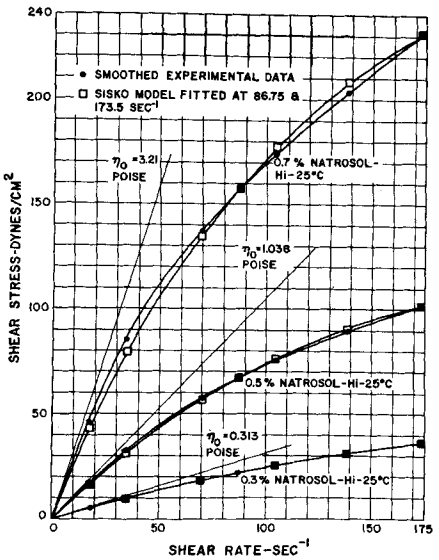

Fig. 4. Comparison of Sisko model with experimental data.

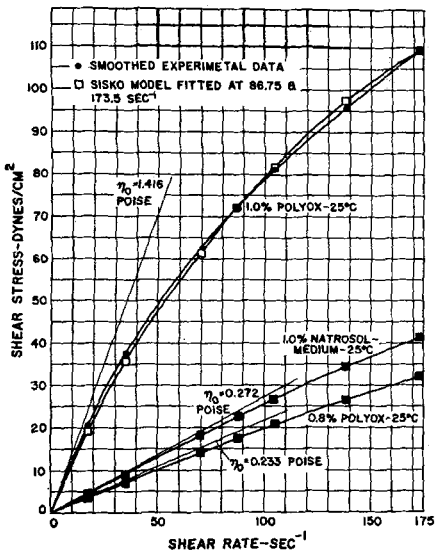

Fig. 5. Comparison of Sisko model with experimental data.

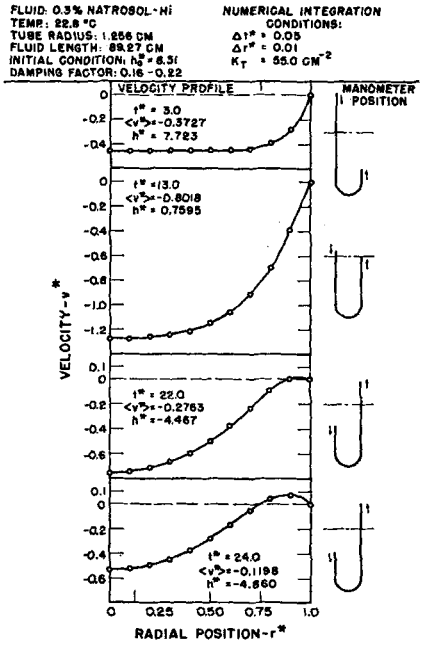

Fig. 6. Velocity profiles, Run 29.

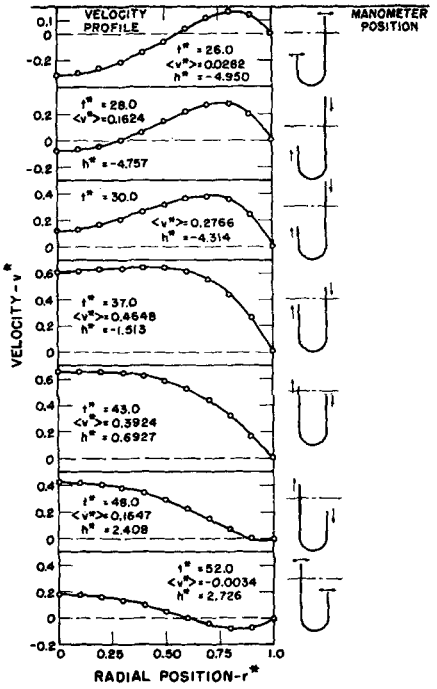

Fig. 7. Velocity profiles, Run 29 (continued).

Because of the increased uncertainty of the rheological curve determination as compared with the Newtonian viscosity determination the error ranges for the non-Newtonian cycle times and damping factors were twice as large as the similar ranges for the Newtonian analysis. The data indicated a consistent error trend for each fluid used. If the polymer solution was stable and was not degrading rapidly with time, each rheological curve produced simulation damping factors in all of the manometer tubes that were consistently high or low when compared with the experimental data. This error trend which persisted in the varying shear rate ranges in the different manometers for a given polymer solution indicated the errors were probably due to the inaccuracy of the rheological curve and not due to visco-elastic effects. As shown in Table 6 the damping factor errors and errors in the η_0 determinations had the same sign and were approximately the same size.

As observed in the Newtonian runs the damping factors for the first cycle with low viscosity fluids were high because of the extra damping due to the reaction force exerted by the high pressure air efflux. The data for these cycles were not included in the overall analysis.

Since the data were greatly influenced by the accuracy of the rheological curve in the low shear rate range, the overall per cycle comparisons were analyzed by combining the runs into three groups. First in group I all of the data were analyzed together. Group II included only the high viscosity solutions of 0.5% Natrosol-Hi, 1.0% Polyox, and 0.7% Natrosol-Hi. In group III all of the data were included except that from Run 27 for 0.8% Polyox and from all of the 1.0% Natrosol-Med runs. These runs were eliminated in this last group in an attempt to remove some of the larger errors due to solution degradation and rheological curve determinations. In Tables 8 and 9 in the Appendix* are summarized the error ranges, average errors, sample standard deviations, sum of squares, and statistical significance tests for the three groups. In the statistical tests the hypothesis that was tested was that the average damping factor or cycle time errors for the

* See footnote on page 552.

TABLE 4. CONSTANTS FOR RHEOLOGICAL MODELS

	Fluid and temperature									
	Natrosol-Hi						Polyox			Natrosol-Med
	0.3%		0.5%		0.7%		0.8%	1.0%		1.0%
Constants*	23.0°C.	25.0°C.	23.0°C	25.0°C.	23.0°C.	25.0°C.	25.0°C.	23.0°C.	25.0°C.	23.0°C.
Sisko model:										
η_0	0.3235	0.313	1.090	1.038	3.78	3.21	0.2325	1.678	1.416	0.2720
$\beta \times 10^5$	994.38	167.14	1788.1	840.10	39527.	21086.	190.78	16022.	8657.5	3.3447
m	1.4712	1.7986	1.6435	1.7732	1.3528	1.4239	1.6283	1.3604	1.4274	2.3359
Oldroyd model:										
η_0	0.3235	0.313	1.090	1.038	3.78	3.21	0.2325	1.678	1.416	0.2720
$\lambda_1^0 \times 10^3$	16.248	12.342	14.718	12.688	22.158	19.695	14.969	22.003	19.589	6.9408
$\lambda_2 \times 10^3$	10.918	6.9688	6.5369	5.4371	6.4596	6.7096	11.137	7.1593	7.3359	5.2379

* Curves fitted to agree with experimental curves at shear rates of 86.75 and 173.5 sec.$^{-1}$. The zero limiting viscosity was determined graphically from the rheological curve.

Newtonian and non-Newtonian data were equal. Included in the tables are the Newtonian data reported previously (*1*). Since the sample standard deviations of the non-Newtonian and Newtonian data differed because of the errors associated with the rheological data, the standard t test had to be modified according to a procedure outlined by Snedecor (*14*).

The data in Tables 8 and 9 indicate that all of the hypotheses, that the Newtonian and non-Newtonian cycle time and damping factor average per cent errors were equal, should be accepted. It is interesting to note that all three groupings of the non-Newtonian data gave average errors which were not significantly different statistically from the Newtonian average error.

The conclusion to be drawn from the above results is that the steady state rheological curves for the non-Newtonian fluids adequately described the behavior of the fluid in this low frequency oscillatory system. No anomalous disagreement between the experimental and simulation data could be found which could be attributed to visco-elastic characteristics of the fluids. In high frequency oscillatory systems experiments have shown that rheological models which include time dependent terms must be used to describe the behavior of the fluid. However the above experiments indicate that the steady state rheological data appear to be adequate in describing behavior of low frequency unsteady state systems.

The above results tend to indicate that if the cycle times of the system are many times greater than the relaxation and retardation times of the fluids utilized, then the steady state data are applicable. In this case the cycle times ranged between 1.5 and 2.0 sec., whereas the retardation and relaxation times from the Oldroyd model ranged between 5×10^{-3} to 22×10^{-3} sec.

Thus for many engineering applications where the frequencies of a physical system are low, designs probably can be made with steady state rheological equations of the Ellis, Sisko, and Eyring type. This simplification of the system equations should lead to more readily utilized design methods, since much steady state rheological data have been taken while little specific information is known about the general visco-elastic equations as applied to specific high polymer solutions.

ACKNOWLEDGMENT

The author wishes to thank Professor R. B. Bird of the University of Wisconsin for his introduction to the oscillating manometer problem. His suggestions and assistance were extremely helpful. Thanks should be given to Professor E. E. Wissler of the University of Texas for loaning the author and Professor Bird a copy of the report describing an undergraduate research project which studied a non-Newtonian oscillating manometer. Also the financial support given by the National Science Foundation during the author's post-doctoral study in the Chemical Engineering Department at the University of Wisconsin was greatly appreciated.

TABLE 5. MANOMETER EXPERIMENTAL RUN CONDITIONS

Run no.	Aqueous solution of:	Fluid Weight %	Temperature, °C.	Density	Fluid length, cm.	Tube inside radius,* cm.
25	Natrosol-Hi	0.5	23.4	1.0	85.82	1.255
26	Natrosol-Hi	0.7	23.4	1.0	84.92	1.255
27	Polyox	0.8	23.5	1.0	89.79	1.256
28	Polyox	1.0	23.4	1.0	89.73	1.256
29	Natrosol-Hi	0.3	22.8	1.0	89.27	1.256
30	Natrosol-Med	1.0	23.5	1.0	89.62	1.256
36	Natrosol-Med	1.0	23.2	1.0	90.82	1.059
37	Natrosol-Hi	0.3	23.3	1.0	91.12	1.059
38	Natrosol-Hi	0.5	22.8	1.0	91.72	1.059
39	Polyox	0.8	23.6	1.0	95.46	1.059
40	Polyox	1.0	23.8	1.0	93.27	1.059
45	Natrosol-Med	1.0	24.1	1.0	92.31	0.4564
46	Natrosol-Hi	0.3	24.2	1.0	94.06	0.4656
47	Polyox	0.8	24.0	1.0	92.44	0.4564

* The tube radius is an average of the radii in the straight and curved sections weighted by the length of fluid in each section.

TABLE 6. AVERAGE DAMPING FACTOR ERRORS VS. POLYMER SOLUTION TYPE

Solution	Average damping factor errors, % 1.25-cm. radius	1.05-cm. radius	0.456-cm. radius	error† of η_0
0.3% Natrosol-Hi	+5	+15	+17	+28
0.8% Polyox	−24*	+2	0	−34*
1.0% Natrosol-Med	+13	+14	+17	+23
0.5% Natrosol-Hi	−9	−1	—	−4.8
1.0% Polyox	−2	0	—	—
0.7% Natrosol-Hi	−11	—	—	−17

* Low due to solution degradation.
† As compared with falling sphere determinations.

NOTATION

F_T = force at ends of liquid legs due to flow reversal, dynes
g_z = acceleration due to gravity in axial direction, cm./sec.^{2}
h_1 = left leg height above initial equilibrium position, cm.
h_2 = right leg height below initial equilibrium position, cm.
h = $(h_1 + h_2)/2$
h^* = dimensionless leg height, h/r_o
K_T = reversal end effect constant, cm.$^{-2}$
L = length of manometer fluid, cm.
L^* = dimensionless length of manometer fluid, L/r_o
m = exponent in Sisko model
P = hydrostatic pressure, dynes/sq.cm.
P^*_T = dimensionless pressure due to flow reversal, $(4/3) \langle v^* \rangle \Omega_2 \eta^*$
r = radial distance from center of tube, cm.
r_o = radius of tube, cm.
r^* = dimensionless radius, r/r_o
R = radius of manometer bend, cm.
s = sample standard deviation
S = cross-sectional area of tube, sq.cm.
t = time, sec.
t^* = dimensionless time, $t[(3/2)g/r_o)]^{1/2}$
v_r = fluid velocity in radial direction
v_θ = fluid velocity in circumferential direction
v_z = fluid velocity in axial direction
v^* = dimensionless velocity, $v[(3/2)r_o g]^{1/2}$
$\bar{x}$ = arithmetic average of % error
z = axial distance in tube, cm.

Greek Letters

ζ = damping factor in second order damped harmonic differential equation
η = non-Newtonian viscosity, poise
η_0 = zero rate of shear limiting viscosity, poise
η^* = dimensionless non-Newtonian viscosity, η/η_0
β = non-Newtonian coefficient in Sisko model, (poise) $(\text{sec.})^{m-1}$
Ω_1 = dimensionless reciprocal zero rate of shear limiting viscosity, $(gr^3_o/24)^{1/2} (\rho/\eta_0)$
Ω_2 = dimensionless flow reversal viscous drag force, $\left(\frac{3r_o}{8g}\right)^{1/2} (K_T \eta_0/\rho)$

Ω_4 = dimensionless Sisko model non-Newtonian viscosity coefficient, = $(r_0^3 g/24)^{1/2}$ (ρ/β) $(2r_0/3g)^{\frac{m-1}{2}}$

λ_1 = stress relaxation time constant in 3 constant Oldroyd model, sec.

λ_2 = rate of shear retardation time constant in 3 constant Oldroyd model, sec.

τ_{rz} = shear stress, force in a direction in plane perpendicular to radial direction, dynes/sq. cm.

τ^*_{rz} = dimensionless shear stress, defined in Equation (9)

$< >$ = average over area of tube

LITERATURE CITED

1. Bird, R. B., W. E. Stewart, and E. N. Lightfoot, "Transport Phenomena," 1 ed., 2 printing, pp. 11-14 and 70, Wiley, New York (1962).
2. Prager, W., "Introduction to Mechanics of Continua," 1 ed., p. 131, Ginn and Company, New York (1961).
3. Smith, T. L., J. D. Ferry, and F. W. Schremp, *J. Appl. Phys.*, **20**, 144 (1949).
4. Markovitz, H., *ibid.*, **23**, 1070-1077 (1952).
5. Oldroyd, J. G., *Proc. Roy. Soc. (London)*, **A245**, 278 (1958).
6. Rivlin, R. S., and J. L. Ericksen, *J. Rat. Mech. and Anal.*, **4**, 323-425 (1955).
7. Biery, J. C., *A.I.Ch.E. Journal*, **9**, 614-619 (1963).
8. Snedecor, G. W., "Statistical Methods," 5 ed., p. 38, The Iowa State College Press, Ames, Iowa (1956).
9. Savant, C. J., Jr., "Basic Feedback Control System Design," 1 ed., p. 9, McGraw-Hill, New York (1958).
10. Biery, J. C., and J. D. Huppler, *Engineering Experiment Station Report No. 16*, University of Wisconsin, Madison, Wisconsin (1962).
11. Williams, M. C., and R. B. Bird, *A.I.Ch.E. Journal*, **8**, 378-82 (1962).
12. Hildebrand, F. B., "Introduction to Numerical Analysis," 1 ed., p. 75, McGraw-Hill, New York (1956).
13. *Ibid.*, p. 198.
14. Snedecor, G. W., *op. cit.*, pp. 97-100.
15. Goldstein, S., ed., "Modern Developments in Fluid Dynamics," Vol. 1, pp. 312-314, Oxford Press, London, England (1950).

Manuscript received March 8, 1963; revision received January 9, 1964; paper accepted January 15, 1964.

Joule-Thomson Effects for Nitrogen-Ethane Mixtures

A. L. STOCKETT and L. A. WENZEL

Lehigh University, Bethlehem, Pennsylvania

In the chemical processing industry it is vital to know enthalpies of gas mixtures for economic designs of thermal equipment. In most cases the lack of reliable data forces one to predict the required values. In the absence of contrary information it is reasonable to expect a mixture to behave similarly to the components of which it is composed. Therefore one normally derives estimates of mixture values by some rule which combines the known enthalpies of the individual components. Methods by which this has been done are well known and have recently been compared by Brewer and Geist (2). It is apparent that only a method which will adequately describe the interactions of different molecular species can be seriously considered as an acceptable combination rule. Thus the problem at hand is essentially twofold: a need for increased knowledge concerning the interaction of unlike molecules, and a need for dependable data with which existing and subsequent theories for predicting mixture results can be checked. The purpose of this research therefore was to provide a useful stepping stone for this large problem.

The authors decided to investigate Joule-Thomson effects for mixtures of nitrogen and ethane in the region straddling the critical states of the components. It was presumed that data taken in this region would allow a severe test of mixture theories to be made. The nitrogen-ethane system provided desirable ranges of temperature (25° to −100°C.) and pressure (up to 2,500 lb./sq.in.) in which to operate. Joule-Thomson effects were chosen to be measured inasmuch as it was required only to measure two intensive properties, temperature and pressure, and these could be measured with a good deal of accuracy. The measurements were sufficient to define the temperature-pressure loci of constant enthalpy from which enthalpy data can be derived. It was necessary to develop a suitable apparatus on which to make these measurements; its description and a discussion of its operation follows. Finally the data obtained are presented, and the results of zero-pressure Joule-Thomson coefficient estimates are discussed.

A. L. Stockett is with Dewey and Almy Chemical Division, W. R. Grace and Company, Cambridge, Massachusetts.

APPARATUS

A flow diagram of the experimental equipment is shown in Figure 1. System gas is drawn from a 2 cu.ft. storage tank through a filter to the diaphragm compressor. This unit is a two-stage, V type of compressor with 3.5 std. cu. ft./min. capacity and maximum discharge pressure of 3,600 lb./sq. in. gauge. This compressor was specifically purchased to eliminate oil contamination previously encountered with a piston compressor. The high-pressure gas passed through a silica gel dryer and then was cooled by returning low-pressure gas in a countercurrent heat exchanger. The precooled gas flowed through a coil of ⅛-in. finned copper tubing immersed in the cryostat bath and was cooled to within 1°C. of the bath temperature.

The cryostat bath fluid was a nonflammable, eutectic mixture of halogenated hydrocarbons (8). It was contained in a stainless steel Dewar of approximately 2 gal. capacity. Cooling of the bath was accomplished by evaporating liquid nitrogen in a submerged heat exchanger. Agitation was provided by a